Research

Separate functional properties of NMDARs regulate distinct aspects of spatial cognition

Erin M. Sanders,[1] Akua O. Nyarko-Odoom,[1] Kevin Zhao,[1] Michael Nguyen,[1] Hong Hong Liao,[1] Matthew Keith,[1] Jane Pyon,[1] Alyssa Kozma,[1] Mohima Sanyal,[1] Daniel G. McHail,[1] and Theodore C. Dumas[1,2]

[1]Krasnow Institute for Advanced Study, George Mason University, Fairfax, Virginia 22030, USA; [2]Psychology Department, George Mason University, Fairfax, Virginia 22030, USA

N-methyl-D-aspartate receptors (NMDARs) at excitatory synapses are central to activity-dependent synaptic plasticity and learning and memory. NMDARs act as ionotropic and metabotropic receptors by elevating postsynaptic calcium concentrations and by direct intracellular protein signaling. In the forebrain, these properties are controlled largely by the auxiliary GluN2 subunits, GluN2A and GluN2B. While calcium conductance through NMDAR channels and intracellular protein signaling make separate contributions to synaptic plasticity, it is not known if these properties individually influence learning and memory. To address this issue, we created chimeric GluN2 subunits containing the amino-terminal domain and transmembrane domains from GluN2A or GluN2B fused to the carboxy-terminal domain of GluN2B (termed ABc) or GluN2A ATD (termed BAc), respectively, and expressed these mutated GluN2 subunits in transgenic mice. Expression was confirmed at the mRNA level and protein subunit translation and translocation into dendrites were observed in forebrain neurons. In the spatial version of the Morris water maze, BAc mice displayed signs of a learning deficit. In contrast, ABc animals performed similarly to wild-types during training, but showed a more direct approach to the goal location during a long-term memory test. There was no effect of ABc or BAc expression in a nonspatial water escape task. Since background expression is predominantly GluN2A in mature animals, the results suggest that spatial learning is more sensitive to manipulations of the amino-terminal domain and transmembrane domains (calcium conductance) and long-term memory is regulated more by the carboxy-terminal domain (intracellular protein signaling).

Experience-dependent activation of N-methyl-D-aspartate receptors (NMDARs) at excitatory synapses in the forebrain enables alterations in excitatory synaptic transmission that contribute to the formation of memory traces (Dumas 2005a). Traditionally, it was thought that NMDAR-dependent synaptic plasticity was controlled entirely by the entry of calcium and its actions as a second messenger in the postsynaptic neuron (Malenka and Bear 2004). More recently it has been shown that, upon binding of glutamate, NMDARs can produce long-term changes in synaptic function independent of calcium conductance (Vissel et al. 2001; Nabavi et al. 2013; Birnbaum et al. 2015; Stein et al. 2015; Li et al. 2016; Dore et al. 2017). Thus, how exactly NMDAR activation contributes to synaptic plasticity and learning and memory remain unclear.

NMDARs are hetero-quatramers containing two obligatory GluN1 subunits and two auxiliary GluN2 subunits. In the forebrain, the auxiliary GluN2 subunits can be both GluN2A, both GluN2B, or one GluN2A and one GluN2B subunit (triheteromeric), depending on the age (Monyer et al. 1994; Al-Hallaq et al. 2007; Rauner and Köhr 2011; Wang et al. 2011) or prior experience of the animal (Chen and Bear 2007; Travaglia et al. 2016; Cercato et al. 2017) or the activity level of the synapse (Fox et al. 2006; Bellone and Nicoll 2007; von Engelhardt et al. 2008; Gambrill et al. 2011). GluN3 subunits are incorporated into NMDARs in the hippocampus and cortex, although this is largely limited to the neonatal period (Pachernegg et al. 2012). Changes in the GluN2 composition of NMDARs alter numerous functional properties, most notably, the degree of calcium conductance through the receptor channel and the ability to directly interact with other synaptic plasticity proteins (Paylor et al. 1996; Stoneham et al. 2010). NMDARs containing GluN2B display reduced open probability and slower deactivation of calcium conductance than receptors containing GluN2A (Chen et al. 1999; Cull-Candy et al. 2001; Erreger et al. 2005). Additionally, GluN2B subunits display greater affinity for calmodulin-dependent protein kinase II (CaMKII) (Barria and Malinow 2005; Petralia et al. 2009), the primary molecule considered necessary for NMDAR-dependent synaptic potentiation (Mayford et al. 1995; Lisman et al. 2002; Hansel et al. 2006; Pi et al. 2010; Sanhueza and Lisman 2013) and RasGRF-1, which acts as a mediator between GluN2B-containing NMDAR activation and LTP or LTD (Li et al. 2006). These "gain-of-function" aspects of GluN2B might suggest that NMDARs containing more GluN2B subunits should better enable spatial cognition. However, while overexpression of GluN2B enhances spatial learning in adult mice (Tang et al. 1999), juvenile animals that naturally express greater levels of GluN2B perform poorly in hippocampal-dependent tasks (Altman et al. 1973; Rudy et al. 1987; Dumas 2005b; Sanders et al. 2013; Travaglia et al. 2016). Additionally, forebrain NMDARs with GluN2A subunits are more closely associated to rapid contextual learning (Sakimura et al. 1995; Kiyama et al. 1998; Bannerman et al. 2008) while NMDARs with GluN2B appear to be more broadly involved in contextual and noncontextual learning and memory (von Engelhardt et al. 2008; Brigman et al.

2010). A better understanding of GluN2 subunit contributions to spatial cognition may be obtained by examining how different signaling modes of NMDARs individually impact spatial learning and memory.

The GluN2 amino acid motifs that regulate calcium conductance are almost entirely in the amino-terminal domain (ATD) and transmembrane domains (TMDs) (Paoletti and Neyton 2007; Gielen et al. 2009; Yuan et al. 2009; Mullasseril et al. 2010), spatially separate from those motifs that enable direct intracellular signaling situated in the carboxy-terminal domain (CTD) (Sala and Sheng 1999; Sheng 2001; Merrill et al. 2005; Prybylowski et al. 2005; Hayashi et al. 2009; Newpher and Ehlers 2009; Sanders et al. 2013). As such, it is possible to apply molecular cloning to selectively alter calcium conductance and intracellular signaling. We created GluN2 chimeras by fusing the ATD and TMDs of GluN2A with the CTD of GluN2B (termed ABc) and, vice versa, by fusing the ATD and TMDs of GluN2B with the CTD of GluN2A (termed BAc). These constructs were integrated into transgenic mice so that we could examine the influence on spatial learning and memory. In adult animals with a predominantly GluN2A background, the presence of the GluN2B CTD is increased in ABc animals, while in BAc animals the ATD and TMDs of GluN2B become overrepresented. Chimera expression was verified in brain sections and mice were tested in spatial and nonspatial versions of the Morris water maze (MWM). Numerous measures supported a spatial learning impairment in BAc animals relative to wild-type (WT) littermates, while ABc animals showed more direct approach to the escape location when tested at 24 h after training. These discoveries are similar to previously results obtained from Y-maze testing where ABc animals displayed measures of a selective enhancement in spatial navigation (Sanders et al. 2013) and suggest that spatial learning is more sensitive to the amino acid composition of the GluN2 ATDs/TMDs and long-term memory is more strongly influenced by intracellular signaling sequences in the GluN2 CTDs.

Materials and Methods

We obtained pCIS-A and pCIS-B plasmids with respective mouse GluN2A and GluN2B full-length cDNA (graciously donated by Dr. Ann Stephenson, University College of London). These plasmids served as templates for PCR amplification of fragments used to generate the chimera injection constructs. We designed mutagenic forward and reverse primers to amplify the ATD + TMDs (amino acids 1–2481 for GluN2A and GluN2B) separately from the CTD (GluN2A: 2482–4512; GluN2B: 2482–4449). The ATD + TMD fragments of GluN2A and GluN2B were separately ligated into pTRE-HA (tet-off) plasmids. Subsequently, the carboxy fragments of GluN2A and GluN2B were serially ligated into pTRE-HA-B$_{ATD+TMD}$ and pTRE-HA-A$_{ATD+TMD}$, respectively. Ligation was performed by SeqWright and final products were completely sequenced. pTRE-HA-ABc (7265 bp) and pTRE-HA-BAc (7494 bp) injection constructs (Fig. 1A) were linearized with AseI and DrdI and sent to the Transgenic Mouse Facility at the University of California, Irvine for oocyte injection. Positive founders (and subsequently their offspring) were bred with mice expressing tTA (tetracycline transactivator) under transcriptional control of the CaMKII minimal promoter (Mayford et al. 1996). Genotyping for tTA and the HA (hemagglutinin) tag sequence on chimeric subunits (Fig. 1B) was performed by PCR on tail snip genomic DNA in-house and, in ambiguous cases, confirmed commercially (Transnetyx).

In situ hybridization

Young adult animals (30–60 d of age) were anesthetized with Isoflurane and perfused with 4% paraformaldehyde (PFA). Brains were removed and stored in PFA for 6 h and then switched to 30% sucrose. Cryopreserved brains were sectioned on a cryostat at 30 μm thickness and stored on magnetic microscope slides
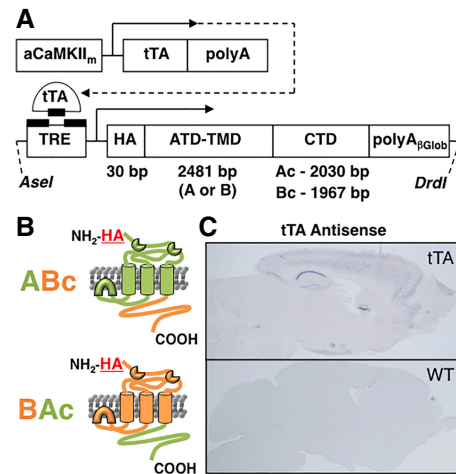
Figure 1. Chimeric GluN2 transgenic design. (*A*) GluN2 chimera expression was regulated by the tet-off transcription system with tTA under transcriptional control of the minimal CaMKII promoter (αCaMKII$_m$) (Mayford et al. 1996). GluN2 chimera injection constructs consisted of the first 2481 bp of GluN2A or GluN2B fused to the CTD of GluN2B (1967 bp) or GluN2A (2030 bp), respectively. A 30-bp sequence coding for HA was inserted in frame upstream of each chimera construct. A β-globin (βGlob) polyadenylation sequence was situated downstream from the chimera construct. (*B*) Illustration of ABc and BAc chimeric subunits situated in a plasma membrane. (*C*) Sagittal brain sections labeled with antisense riboprobe targeting tTA mRNA. (*Top*) Labeled section collected from an tTA/ABc double-positive mouse. (*Bottom*) Labeled section collected from a WT mouse.

(SuperFrost Plus, Fisher Scientific) at −70°C. In vitro transcription reactions were performed (DIG RNA Labeling Kit, Roche) to produce a 760 bp riboprobe that was antisense to tTA (tTA template plasmid was a kind gift from Dr. Clifford Kentros). Specific single-stranded riboprobe products were confirmed by standard agarose electrophoresis run in Tris–borate–EDTA (TBE) buffer.

Riboprobe was diluted in hybridization buffer (PerfectHyb Plus, Sigma-Aldrich) and denatured at 70°C. Denatured probe was applied to prewarmed tissue sections and incubated overnight (62°C). The following day, excess probe was removed by washing with SSC-(50%) formamide followed by maleic acid buffer (MABT, 100 mM maleic acid, 15 mM NaCl, 0.2% Tween-20) at 62°C. Tissue was then treated with blocking solution (MABT, 10% sheep serum, 2% blocking reagent) for 1 h at room temperature (RT) and incubated in anti-dig antibody (1:1500, fab fragments, Roche). Excess antibody was removed by washing with MABT followed by alkaline phosphatase (AP) staining buffer (100 mM NaCl, 50 mM MgCl$_2$, 100 mM Tris, 0.1% Tween-20, pH 9.5) and the tissue was then transferred to staining solution (AP staining buffer with 10 % 100 kDa polyvinyl alcohol, 10 mM Levamisol, 3.5 μL/mL NBT, and 2.6 μL/mL BCIP in AP staining buffer) and incubated at 37°C for 4 h. The color reaction was stopped by washing with phosphate buffered saline (PBS) containing Triton X-100 (0.1%) at RT. Finally, tissue sections were dehydrated through ascending alcohol concentrations, defatted with xylenes, and coverslipped. Bright field images were captured at 2×–20× magnification.

Immunohistochemistry

Translation of chimeric GluN2 NMDAR subunits and translocation to synapses was assessed with immunohistochemistry (IHC). Brains from adult ABc, BAc, and WT animals were harvested and cryopreserved as stated for in situ hybridization (ISH). Sagittal sections were cut on a vibratome at 30 μm and processed according to a free-floating IHC protocol. Slices were permeabilized with 0.1% Triton-X and pretreated with sodium borohydride (2 ng/mL in sterile water) to minimize tissue autofluorescence. Sections were

washed in PBS and blocked with normal goat serum (1% NGS, 0.1% Triton X-100 in PBS) at RT for 1 h. Sections were washed again in PBS and incubated for 72 h in blocking solution containing primary antibody at 4°C. Anti-HA (1:450 dilution; rabbit polyclonal, Rockland) was coapplied with α-PSD95 (1:450 dilution; mouse monoclonal, Thermo Fisher Scientific) or α-SAP102 (1:450 dilution; mouse monoclonal, Rockland) primary antibodies. Slices were subsequently washed with PBS and incubated in blocking solution containing secondary antibodies (1:2500 dilution; α-rabbit-fluorescein, and α-mouse-Cy3, Jackson ImmunoResearch) for 4 h at RT. After final PBS washes, slices were mounted on glass microscope slides and coverslipped in Vectashield (Vector Laboratories) with DAPI.

Fluorescent signal intensities for HA, PSD95, and SAP102 were imaged by confocal microscopy (C1 Plus, Nikon) at 20×, 40×, and 60×. To remove residual autofluorescence signals, laser power and signal gain levels for each channel were set to produce almost no signal on sections that were exposed to secondary antibody, but no primary antibody. These settings were then applied to all sections treated with primary antibody from all genotype groups. For analysis, raw data values were compared by two-way ANOVA (genotype × synaptic region). Signal intensities for all groups were normalized to mean signal intensities recorded from WT tissue sections and presented as normalized intensities.

MWM training

Animals were trained on spatial version of the MWM. The testing environment was spatially enriched with various groups of black shapes hanging on white curtains surrounding roughly three quarters of the pool circumference and an off-white wall and bio-containment hood visible through the curtain gap. The pool was black with a diameter of 127 cm. The platform diameter was 17.5 cm. The pool water was made opaque with nontoxic white tempera paint and maintained at a temperature of 24°C. The platform was painted white and positioned 1 cm below the water surface. The escape platform remained at one goal location across all training trials for each animal, but shifted between cohorts. Animals from each genotype were trained in a counter-balanced order and all genotypes were represented in each testing cohort. Also, the goal location was moved to a new location for each testing cohort so that each quadrant was represented similarly in the final analyses.

A 1-d massed training protocol was performed. Just prior to the first trial, naïve animals were pretrained by being allowed climb onto the platform from three different directions and sit for 10 sec each time. Immediately following climbing practice, escape training ensued. Escape training consisted of five blocks of three escape trials (15–20 min inter-block interval) followed by a single probe trial (immediate, IMM), to test for spatial learning, and then three more "refresher" escape trials (refresher trials were not included in data analyses). A single long-term memory probe was performed 24-h following training to assess spatial memory. For each trial, the animal was placed at one of four starting positions varied pseudorandomly along the edge of the pool (starting positions were offset from goal locations by 45°). Training trials lasted for 1 min or until the animal reached the goal platform. If the platform was not found, the animal was guided onto the platform. In either case, the animal remained on the escape platform for 15 sec. For the probe trials, the platform was removed from the pool. The animals were started at one of two "far" locations 73 cm from the center of the goal location and allowed to search for 1 min. After each training block or probe trial, animals were gently toweled off and placed in a heated cage (~29°C) until dry and then returned to the home cage to wait for the next trial block.

In a separate test with separate subjects, a nonspatial escape task was performed. In this case, the curtains were rolled up to minimize the extramaze cues, the pool water was clear, and a white wiffle ball was attached to the center of the escape platform. The escape platform was moved to a new quadrant for each trial within a testing block and across testing blocks in a pseudorandom order. The start location was also moved for each trial as was performed for the spatial version of the MWM. Twenty-four hours following

training, three additional trials were performed to test long-term memory.

For both versions of the MWM test, animal position was continually tracked during training and probe trials by an overhead video camera and tracking software (MazeScan, CleverSys Inc.). Escape latencies were measured by stopwatch. Path length and swim speed were extracted from each training trial and averaged by training block to create learning curves for each animal. Dwell time in each quadrant, time spent over goal location, and distance from platform (1 Hz sampling rate) were calculated for each probe trial for every animal. Two-way repeated-measures ANOVAs (genotype × training block) were used to compare learning curves. Goal quadrant biases for probe trials were calculated within groups by χ^2 test. Dwell time in the goal quadrant and time over goal location were analyzed by one-way ANOVA. Directness of initial approach was analyzed by two-way repeated measures ANOVA (genotype × sample time). Where necessary (violation of Mauchly's test for sphericity), the Greenhouse–Geisser correction was applied to the two-way ANOVAs. Tukey HSD post hoc tests were used to determine individual group differences.

Results

In situ hybridization

Colorimetric ISH using an antisense probe targeting tTA produced punctate labeling of cell bodies in forebrain regions only (Fig. 1C). tTA expression was observed in the neocortex and hippocampus, but not in the striatum or olfactory bulb. Expression was most dense in area CA1 of the hippocampus and sparse in all other hippocampal and cortical regions.

Immunohistochemistry

Confocal images were taken from sagittal brain sections collected from young adult ABc, BAc, and WT mice treated with primary antibodies targeting HA, SAP102, and PSD95 (example images shown in Fig. 2A). Signal intensities for HA, SAP102, and PSD95 were measured in three dendritic fields (CA1 stratum radiatum, RAD; CA1 stratum moleculare, MOL; dentate gyrus stratum moleculare, DG) and compared across genotype (ABc, BAc, WT). Across all hippocampal areas, there was a main effect of genotype on HA signal intensity [$F_{(2,60)} = 10.83$, $P < 0.001$], reflecting the presence of ABc (versus WT, $P < 0.001$) and BAc (versus WT, $P < 0.005$) subunits. Within anatomical region, there was an effect of genotype on HA levels in the RAD [one-way ANOVA, $F_{(2,18)} = 4.33$, $P < 0.05$], the MOL [$F_{(2,18)} = 4.27$, $P < 0.05$], and the DG [$F_{(2,18)} = 5.19$, $P < 0.02$]. Relative to WTs, HA signal was elevated in both ABc (RAD, $P < 0.006$; MOL, $P < 0.001$; DG, $P < 0.002$) and BAc sections (RAD, $P < 0.006$; DG, $P < 0.004$) (Fig. 2B).

There were no main effects of genotype or region or an interaction effect on SAP102 signal intensities. In contrast, there was a main effect of genotype on PSD95 expression [$F_{(2,36)} = 11.92$, $P < 0.0001$]. Within regions, there was a main effect of genotype for the RAD [$F_{(2,11)} = 4.40$, $P < 0.05$] and in the DG [$F_{(2,11)} = 4.29$, $P < 0.05$]. Post hoc analyses showed that the significant differences were carried entirely by ABc animals. For ABc animals, PSD95 expression was elevated relative to WT in RAD ($P < 0.049$) and DG ($P < 0.048$) (Fig. 2B) with a trend for significance in MOL ($P = 0.057$). PSD95 expression in sections from BAc mice was not different from WTs in any region. Considering all IHC results together, the data indicate that 1) ABc and BAc subunits are expressed and translocated into dendrites in area CA1 and in the DG and 2) ABc expression is accompanied by an increase in PSD95 expression.

Spatial MWM—training trials

During the training phase, when analyzing all five blocks, escape latencies decreased across training blocks [$F_{(4,292)} = 26.0$,
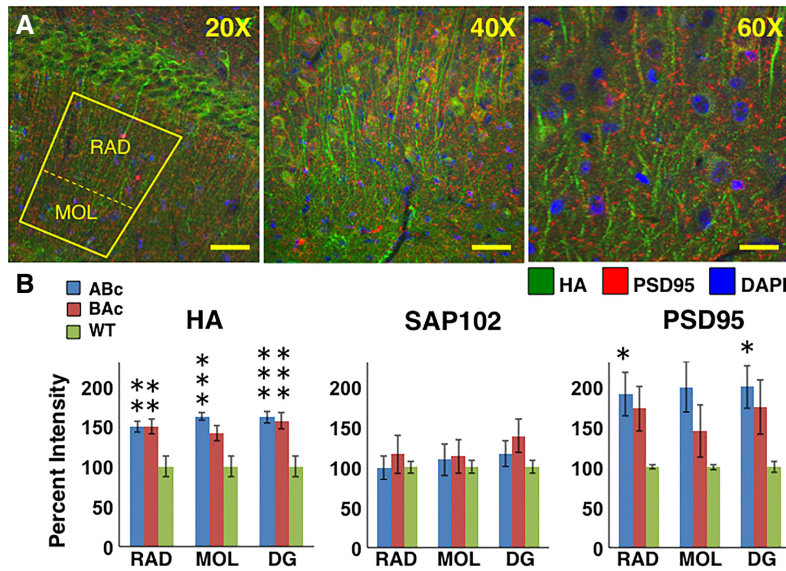
Figure 2. IHC for GluN2 chimeric subunits and synaptic anchoring proteins. (*A*) Representative image of colabeling for HA (green) and PSD95 (red) and stained with DAPI (blue) in 30 µm hippocampal slice of an ABc chimeric mouse (shown at 20×, 40×, and 60× magnification). Yellow boxes illustrate boundaries for extraction of average signal intensities for stratum radiatum (RAD) and stratum moleculare (MOL). Yellow lines are scale bars: 20×, 60 µm; 40×, 30 µm; 60×, 20 µm. Intensities were also extracted from the stratum moleculare of the dentate gyrus (DG). (*B*) Quantification of signal intensities for HA (*n* = 4 animals per genotype), PSD95 (*n* = 6 animals per genotype), and SAP102 (*n* = 6 animals per genotype) antibodies applied to sections from ABc, BAc, and WT mice. Both transgenic lines expressed chimeric subunits (increased HA signal). SAP102 expression was not altered compared to WT animals. ABc expression increased PSD95 expression in the RAD and DG. Statistical significance versus WTs is indicated as follows: (*) $P < 0.05$, (**) $P < 0.01$, and (***) $P < 0.005$.

$P < 0.0001$], but there was no main effect of genotype [$F_{(2,73)} = 2.06$, $P = 0.14$] and no genotype by block interaction [$F_{(8,292)} = 0.67$, $P = 0.72$] (Fig. 3A). Given that GluN2A knockout mice display a selective impairment in rapid contextual learning (Sakimura et al. 1995; Kiyama et al. 1998; Bannerman et al. 2008), we eliminated the final two testing blocks from the analysis to test for an effect of GluN2 chimera expression on learning rate. When only the first three blocks were analyzed, a main effect of genotype emerged [$F_{(2,73)} = 3.93$, $P = 0.02$], but no genotype by block interaction [$F_{(4,146)} = 0.41$, $P = 0.80$] (Fig. 3A). Escape latencies were greater for BAc mice compared to WTs (Tukey HSD, block 2: $P < 0.019$), suggesting slower initial learning in the BAc animals.

The mean path length from the start location to the escape platform varied across block [$F_{(4,64)} = 3.31$, $P = 0.02$], but there was no effect of genotype [$F_{(2,16)} = 0.09$, $P = 0.91$] and no genotype by block interaction [$F_{(8,64)} = 1.21$, $P = 0.31$] (Fig. 3B). When the analysis was restricted to the first three blocks, there was no effect of genotype [$F_{(2,56)} = 1.36$, $P = 0.28$] or block [$F_{(2,56)} = 1.97$, $P = 0.16$] and there was no genotype by block interaction [$F_{(4,56)} = 0.55$, $P = 0.70$]. Swim speed analysis across all five training blocks revealed no main effect of training block [$F_{(4,64)} = 0.37$, $P < 0.77$] or genotype [$F_{(2,16)} = 1.76$, $P = 0.20$] and no genotype by block interaction [$F_{(8,64)} = 0.92$, $P < 0.51$] (Fig. 3C), suggesting no effect of GluN2 chimera expression on swimming ability and no modulation of swimming ability across training trials. Combined, the data support a normal rate of escape learning in adult ABc mice, but slower escape learning in BAc animals.

Spatial MWM—immediate probe trial

During the immediate probe trial, WT and ABc animals similarly showed significant goal quadrant biases (WT: $\chi^2 = 13.76$, $P < 0.005$; ABc: $\chi^2 = 11.96$, $P < 0.01$), while BAc mice showed no bias

($\chi^2 = 3.3$; $P = 0.34$) (Fig. 4A) further supporting an impairment in spatial learning in the BAc line. Examination of the goal quadrant alone revealed no difference in dwell time across genotypes [one-way ANOVA: $F_{(2,64)} = 2.08$, $P = 0.13$] (Fig. 4B). However, time spent over the goal location was impacted by genotype [$F_{(2,64)} = 3.78$; $P < 0.05$], where BAc animals spent less time over the goal location compared to WT animals (Tukey HSD, $P < 0.05$) (Fig. 4C). Combined with the lack of a genotype effect on goal quadrant latency, this result suggests that a coarse spatial navigation capacity is present in the BAc animals, but the ability to locate the escape location is less accurate. While a standard measure, goal quadrant dwell time is a relatively poor way to assess spatial search strategy (animals spend time scratching on the pool wall in the goal quadrant and this quadrant is often abandoned within tens of seconds after an unsuccessful search). Proximity measures, such as the distance-to-platform measure developed by Gallagher et al. (1993), have been compared to other analyses and deemed superior for detecting group differences in spatial memory ability (Pereira and Burwell 2015; Kapadia et al. 2016). Analysis of directness of initial approach toward the goal location (proximity sampled at 1 Hz during the first 10 sec)
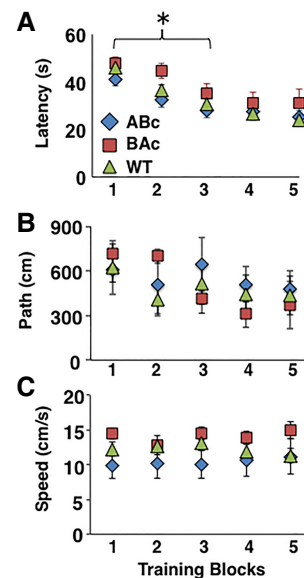
Figure 3. Learning performance across training blocks. (*A*) Mean escape latency (Latency) across training blocks for all genotypes. BAc chimeras took longer to reach the platform across the first three training blocks. ABc (*n* = 25), BAc (*n* = 14), and WT (*n* = 37). (*B*) Mean path length to escape (Path) across training blocks. There was a main effect of training block, but no main effect of genotype on path length. ABc (*n* = 7), BAc (*n* = 7), and WT (*n* = 5). (*C*) Mean swim speed (Speed) across training blocks. There was no main effect of training block or of genotype on swim speed. Statistical significance versus WTs: (*) $P < 0.05$.
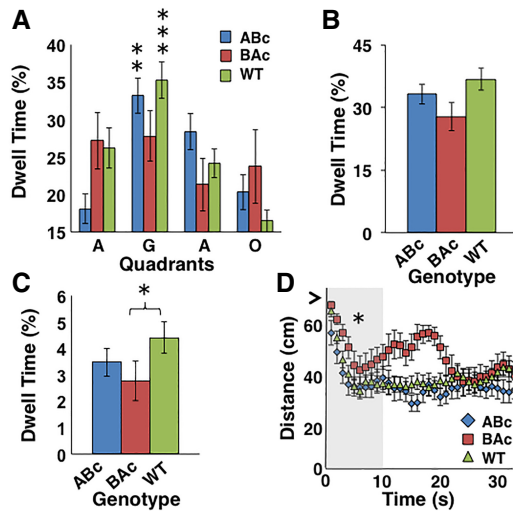
Figure 4. Spatial performance in the IMM probe. (*A*) Mean dwell time across all quadrants for all genotypes (quadrants: [G] goal; [O] opposite quadrant; [A] adjacent). ABc (*n* = 25), BAc (*n* = 14), and WT (*n* = 37). (******) *P* < 0.01, and (*******) *P* < 0.005. Only BAc chimeras did not have a goal quadrant bias. (*B*) Mean dwell time in the goal quadrant for all genotypes. There was no effect of genotype on goal quadrant dwell time. (*C*) Normalized mean dwell time over the goal location during the immediate probe for all genotypes. BAc chimeras spent less time over goal location than WTs, (*****) *P* < 0.05. (*D*) Mean distance to goal location sampled at 1 Hz was calculated for each genotype. Start location distance is marked by a black arrowhead on the *Y*-axis. The first 10 sec were analyzed to measure directness of approach to the goal location. BAc chimeras were consistently farther away from goal location than the WT animals, (*****) *P* < 0.05.

revealed significant effects of sample time [$F_{(9,594)} = 33.02$, $P < 0.0001$] and genotype [$F_{(2,66)} = 3.54$, $P < 0.04$], but no genotype by sample interaction [$F_{(2,66)} = 1.19$, $P < 0.27$]. BAc animals exhibited greater distance to platform values than WT (Tukey HSD, sample times 2–6, 9: $P < 0.05$) (Fig. 4D). There was no genotype effect on swim speed [ABc: 16.3 ± 1.5 cm/sec; BAc: 16.8 ± 0.6 cm/sec; WT: 16.9 ± 1.0 cm/sec; $F_{(2,66)} = 1.18$; $P = 0.31$] [$F_{(2,72)} = 0.06$, $P = 0.94$]. Overall, results from four separate measures (escape latency early in training, goal quadrant bias, time over platform, and distance to platform during the probe trial) support a reduced proficiency in learning the location of or in executing a route to the goal location for the BAc, but not the ABc mice.

Spatial MWM—24-h probe trial

A massed training protocol for the MWM produces suboptimal learning and memory compared to spaced training (Commins et al. 2003; Vorhees and Williams 2014). As a result, only WT animals displayed a significant quadrant bias during the 24-h probe ($\chi^2 = 13.56$, $P < 0.005$) (Fig. 5A). Analysis of dwell time within the goal quadrant alone revealed no effect of genotype [$F_{(2,66)} = 0.84$, $P = 0.44$] (Fig. 5B). Analyzing time over goal location revealed a significant genotype effect [$F_{(2,60)} = 3.22$, $P < 0.05$]. BAc mice spent less time over the goal location ($P < 0.05$) compared to WTs (Fig. 5C). Also, there were significant main effects of sample time [$F_{(9,639)} = 22.97$, $P = 0.0001$] and genotype [$F_{(2,71)} = 6.24$, $P < 0.005$] but no genotype by sample time interaction [$F_{(18,639)} = 1.00$, $P = 0.46$] (Fig. 5D). BAc mice showed larger mean values (Tukey HSD, sample time 6–10: $P < 0.01$) for distance to platform than WTs across the first 10 sec. This result was expected due to the learning impairment observed during training and the search performance deficit during the immediate probe trial. In sharp

contrast, ABc animals exhibited reduced distance to platform values compared to WT ($P < 0.05$) or BAc mice ($P < 0.005$), indicating a more direct approach to the goal location (Fig. 5D). There was no genotype effect on swim speed [ABc: 19.3 ± 1.8 cm/sec; BAc: 20.8 ± 0.8 cm/sec; WT: 20.0 ± 1.0 cm/sec; $F_{(2,69)} = 0.21$; $P = 0.81$] [$F_{(2,69)} = 0.21$, $P < 0.81$]. Together, these data support a possible enhanced ability of the ABc mice to orient to space or plan a route to the goal location when tested a day after training.

Nonspatial MWM

In a single day, each animal performed 18 training trials separated into six blocks with a nonstationary escape platform marked with a white wiffle ball. Similar to the spatial version of the MWM, mean escape latencies (Fig. 6A) and path lengths (Fig. 6B) decreased across training blocks [latency: $F_{(5,125)} = 19.17$, $P = 0.0001$; path length: $F_{(5,125)} = 20.32$, $P = 0.0001$] (Fig. 5). There was no main effect of genotype on escape latency [$F_{(2,25)} = 1.06$, $P = 0.36$] or path length [$F_{(2,25)} = 0.46$, $P = 0.63$]. There were also no genotype by training block interactions for any measure [escape latency: $F_{(10,125)} = 0.73$, $P = 0.61$]; path length: $F_{(10,125)} = 1.54$, $P = 0.20$]; swim speed: $F_{(10,125)} = 0.57$, $P = 0.78$]. To compare more directly to the results from the spatial test, the repeated measures analysis was restricted to the first three blocks. Unlike the spatial test, when the analysis was restricted to the first three blocks, there was no effect of genotype on escape latency [$F_{(2,83)} = 1.10$, $P = 0.35$] or path length [$F_{(2,83)} = 0.91$, $P = 0.41$] but there was an effect of training block [escape latency: $F_{(2,83)} = 14.50$, $P = 0.0001$; path length: $F_{(2,83)} = 12.60$, $P = 0.0001$]. There were no genotype by block interactions on escape latency [$F_{(4,83)} = 0.78$, $P = 0.54$] or path length [$F_{(4,83)} = 1.82$, $P = 0.14$]. When swim speed was
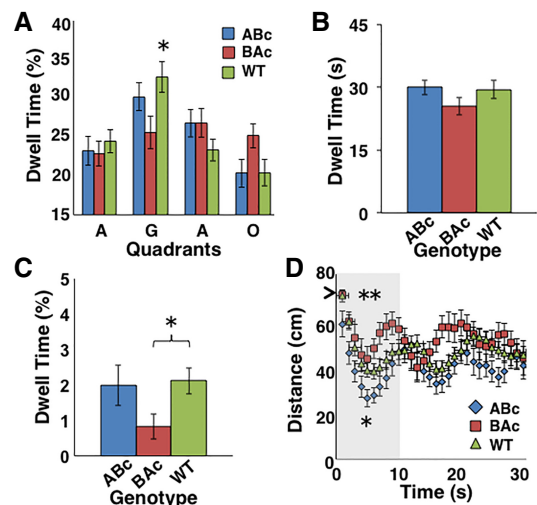
Figure 5. Long-term spatial memory in the MWM. (*A*) Mean dwell time across all quadrants for all genotypes during the 24-h probe (quadrants: [G] goal; [O] opposite quadrant; [A] adjacent). ABc (*n* = 22), BAc (*n* = 14), and WT (*n* = 29). Only WT animals displayed a goal quadrant bias (significant χ^2 result, (*****) *P* < 0.05). (*B*) Mean dwell time in the goal quadrant for all genotypes. There was no effect of genotype on goal quadrant dwell time. (*C*) Mean time spent over goal location during the 24-h probe for all genotypes. BAc chimeras spent less time over goal location than WT animals, (*****) *P* < 0.05. (*D*) Mean distance to goal location sampled at 1 Hz was calculated for each genotype. Start location distance is marked by a black arrowhead on the *Y*-axis. The first 10 sec were analyzed to measure directness of approach to the goal location. BAc chimeras were consistently farther away from goal location than the WT animals, (******) *P* < 0.01. ABc mice approached the platform more directly than WTs, (*****) *P* < 0.05.
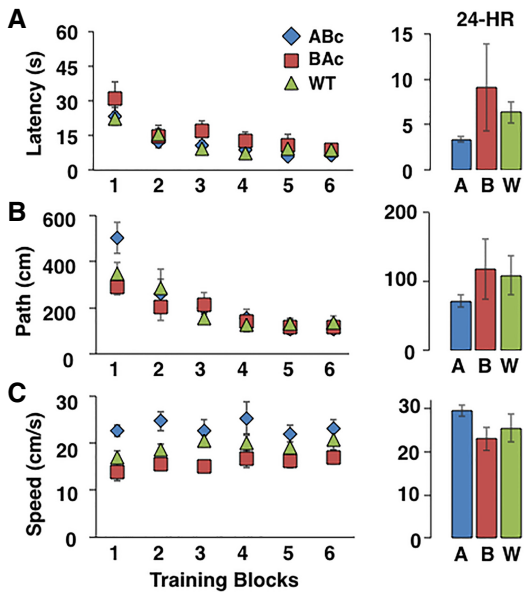
Figure 6. Learning performance across training blocks in the nonspatial escape task. (*A*) Mean escape latency (Latency) across training blocks for all genotypes. There was a main effect of training block, but no effect of genotype on path length. ABc (*n* = 8), BAc (*n* = 8), and WT (*n* = 10). (*B*) Mean path length to escape (Path) across training blocks. There was a main effect of training block, but no effect of genotype on path length. (*C*) Mean swim speed (Speed) across training blocks. There was no main effect of training block, but there was an effect of genotype on swim speed. There was no effect of genotype on escape latency, path length, or swim speed during the 24-h tes. A = ABc, B = BAc, and W = WT.

analyzed across all five training blocks, there was a main effect of genotype [$F_{(2,25)}$ = 5.76, P = 0.01], but no effect of training block [$F_{(5,125)}$ = 1.67, P = 0.17] and no genotype by training block interaction [$F_{(10,125)}$ = 1.54, P = 0.20] (Fig. 6C). These results did not change when only the first three blocks were analyzed [genotype: $F_{(2,83)}$ = 8.97, P = 0.002; training block: $F_{(2,83)}$ = 2.50, P = 0.09; interaction: $F_{(4,83)}$ = 0.97, P = 0.43]. ABc animals swam consistently faster across training blocks (Tukey HSD, blocks 1 and 2: P < 0.05). Combined, these data suggest no impact of GluN2 chimera expression on cued escape learning.

When tested 24-h after initial training, there were no group differences in mean escape latency [$F_{(2,25)}$ = 0.99, P = 0.39], path length [$F_{(2,25)}$ = 0.54, P = 0.59], or swim speed [$F_{(2,25)}$ = 1.09, P = 0.35] (Fig. 6, right), supporting no effect of GluN2 chimera expression on nonspatial long-term memory.

Discussion

We verified transgene expression in forebrain principle cells, documented transgene translation to protein, and quantified translocation of NMDARs with chimeric subunits into dendrites. By expressing chimeric GluN2 subunits in NMDARs at hippocampal synapses in adult animals, we were able to show that different receptor properties likely affect separate aspects of spatial cognition. BAc animals displayed slower and perhaps less accurate learning while ABc animals exhibited an enhanced ability to orient to the goal location when tested at 24-h after training. Both mutant groups were not distinguishable from WTs in a nonspatial water escape task supporting selective spatial effects of GluN2 chimera expression in the forebrain. Largely different behavioral results were obtained from the ABc and BAc lines that use the same transcription system, suggesting that the effects were not a nonspecific re-

sult of transgene overexpression and strongly support an effect of amino acid sequence.

We interpret the molecular basis of the behavioral outcomes with respect to native GluN2 subunit background in adult WT animals. Synaptic NMDARs containing two GluN2B subunits are lost during postnatal development and replaced by NMDARs with two GluN2A subunits or one GluN2A and one GluN2B subunit (Barria and Malinow 2002; Al-Hallaq et al. 2007). Thus, in mature animals, the GluN2 background is predominantly GluN2A. In our BAc animals, the contrast to the WT background is the ATD and TMDs of GluN2B. These animals display a reduced capacity for spatial learning. Since the ATD and TMDs regulate calcium conductance, these results suggest that GluN2B-type calcium conductance is not optimal for spatial learning. Conversely, in the ABc animals, the contrast to the WT background is the GluN2B CTD. These animals outperform BAc and WT animals at the start of the long-term spatial memory test. Since the CTD provides the metabotropic signaling, this finding implicates the GluN2B CTD metabotropic signaling as a positive modulator of memory processes (consolidation, maintenance, or retrieval). Alternatively, ABc expression results in removal of the GluN2A CTD, which has been shown to be a negative modulator of memory maintenance (Sprengel et al. 1998; Shinohara and Hata 2018). Regardless, separate signaling properties of NMDARs likely make independent contributions to different aspects of spatial cognition. This conclusion will be further explored by direct measurement of NMDAR-dependent calcium currents recorded from CA1 pyramidal neurons in hippocampal slices and through immunohistochemical quantification of calcium-independent NMDAR signaling in maze-tested animals.

GluN2 chimeras have been engineered into transgenic mice by other investigators to study the neural bases of learning and memory. Analogous to our results in a spatial task, adult mice expressing ABc chimeric GluN2 subunits display long-term memory for novel objects that is superior to WTs (Jacobs et al. 2014) and BAc-type chimeras display impaired long-term memory for fearful (Jacobs et al. 2014) and social events (Jacobs et al. 2015). Likewise, in knock-in mice, BAc equivalent animals displayed impaired contextual fear conditioning, but there was no effect of the ABc knock-in (Ryan et al. 2013). As such, while similar effects have been reported previously, the current results illustrate the learning impairment produced by overexpression of the GluN2B ATD and TMDs and the cognitive enhancement produced by overexpression of the GluN2B CTD in BAc and ABc mice performing the same behavioral task. The cognitive enhancement was likely made visible by the more difficult massed training protocol (leaving room for improvement). Application of a spaced training protocol and intermittent probe trials might discern between possible effects on the facility of memory consolidation or the total capacity for long-term memories.

More recent studies involving expression of GluN2 chimeras and GluN2 subunits with CTD deletions have shown independent involvement of the carboxy tails of GluN2A and GluN2B in LTP induction (Köhr et al. 2003; Berberich et al. 2007; Foster et al. 2010). In hippocampal slices prepared from adult mice having native GluN2A subunits replaced with GluN2A subunits lacking the CTD, LTP magnitude was reduced and LTP induction was abolished by treatment with antagonists that block GluN2B-containing NMDARs (Köhr et al. 2003). Thus, alternative to the formerly held notion that GluN2A and GluN2B, as whole subunits, regulate different forms of plasticity (Liu et al. 2004; Massey et al. 2004; Izumi et al. 2006), a newer, more plausible idea is that functional domains of GluN2A and GluN2B act together to facilitate plasticity induction. Specifically, the combination of ATD and TMDs of GluN2A and the CTD of GluN2B optimized maze performance, potentially through greater temporal control over the rise in the level of intracellular calcium (GluN2A) working together with greater

recruitment of critical plasticity proteins, like CaMKII or RasGRF-1 (GluN2B).

Triheteromeric NMDARs contain one GluN2A subunit and one GluN2B subunit and display calcium conductance properties that are intermediate to diheteromeric NMDARs with GluN2A and GluN2B (Monyer et al. 1992; Rauner and Köhr 2011). Prior studies point to higher proportions of triheteromeric NMDARs at mature versus less mature glutamatergic synapses in the hippocampus (Al-Hallaq et al. 2007; Rauner and Köhr 2011; Wang et al. 2011), though developmental changes in synaptic content of triheteromeric NMDARs have not been studied directly. To consider how triheteromeric NMDARs play a role in our transgenic lines, we made a diagram to propose ABc and BAc contributions in di- and triheteromeric receptors (Fig. 7). Assuming complete transformation where both native GluN2 subunits are replaced by chimeric GluN2 subunits within a receptor, the molecular outcome is the same for synapses with diheteromeric or triheteromeric NMDARs. The situation is more complicated for a single subunit replacement in triheteromeric NMDARs because the chimeric subunit may replace either the GluN2A or GluN2B subunit. Thus, in the ABc line showing long-term memory enhancement, if ABc subunits selectively replace GluN2B subunits, the already dominant GluN2A-type ATD and TMD representation increases. If ABc subunits selectively replace GluN2A subunits, the GluN2B-type CTD representation increases. Given a high level of GluN2A content in adults, the former replacement possibility (ABc for GluN2B) is less plausible in explaining the cognitive enhancement.

Positioning of NMDARs adjacent to presynaptic release sites is reliant on specific anchoring proteins in the postsynaptic density, including PSD95 and SAP102 (Sans et al. 2000, 2003; Béïque et al. 2006; Besshoh et al. 2007; Elias et al. 2008; Minatohara et al. 2013). Prior sequential immunoprecipitation studies have shown similar affinities of GluN2A and GluN2B for PSD95 and SAP102 in adult hippocampal homogenates (Al-Hallaq et al. 2007). Our immunohistochemical results revealed elevations in dendritic content of PSD95, but not SAP102, only in the ABc line. Thus, behavioral alterations could be related to increased synaptic content of PSD95, a related increase in total number of NMDARs per synapse, or an increase in the number of synapses. These possibilities can be addressed in part through morphological studies that quantify dendritic spines and through electrophysiology. However, as stated above, the behavioral outcomes of ABc and BAc expression are very different and not likely explained by a secondary alteration that is common to both lines.

In summary, the current studies indicate that manipulations in calcium conductance or intracellular signaling domains of NMDARs produce separable alterations in hippocampal-dependent behaviors in mature mice. The findings support further submolecular analyses and interdisciplinary studies of NMDAR function across the lifespan. Findings from such studies could enable the production of improved treatments for developmental and adult disorders where NMDARs are implicated, including Fragile X syndrome, autism spectrum disorders, and schizophrenia (Lau and Zukin 2007).

Acknowledgments

References

Al-Hallaq RA, Conrads TP, Veenstra TD, Wenthold RJ. 2007. NMDA di-heteromeric receptor populations and associated proteins in rat hippocampus. *J Neurosci* **27:** 8334–8343.

Altman J, Brunner RL, Bayer SA. 1973. The hippocampus and behavioral maturation. *Behav Biol* **8:** 557–596.

Bannerman DM, Niewoehner B, Lyon L, Romberg C, Schmitt WB, Taylor A, Sanderson DJ, Cottam J, Sprengel R, Seeburg PH, et al. 2008. NMDA receptor subunit NR2A is required for rapidly acquired spatial working memory but not incremental spatial reference memory. *J Neurosci* **28:** 3623–3630.

Barria A, Malinow R. 2002. Subunit-specific NMDA receptor trafficking to synapses. *Neuron* **35:** 345–353.

Barria A, Malinow R. 2005. NMDA receptor subunit composition controls synaptic plasticity by regulating binding to CaMKII. *Neuron* **48:** 289–301.

Béïque JC, Lin DT, Kang MG, Aizawa H, Takamiya K, Huganir RL. 2006. Synapse-specific regulation of AMPA receptor function by PSD-95. *Proc Natl Acad Sci* **103:** 19535–19540.

Bellone C, Nicoll RA. 2007. Rapid bidirectional switching of synaptic NMDA receptors. *Neuron* **55:** 779–785.

Berberich S, Jensen V, Hvalby Ø, Seeburg PH, Kohr G. 2007. The role of NMDAR subtypes and charge transfer during hippocampal LTP induction. *Neuropharmacology* **52:** 77–86.

Besshoh S, Chen S, Brown IR, Gurd JW. 2007. Developmental changes in the association of NMDA receptors with lipid rafts. *J Neurosci Res* **85:** 1876–1883.

Birnbaum JH, Bali J, Rajendran L, Nitsch RM, Tackenberg C. 2015. Calcium flux-independent NMDA receptor activity is required for Aβ oligomer-induced synaptic loss. *Cell Death Dis* **6:** e1791.

Brigman JL, Wright T, Talani G, Prasad-Mulcare S, Jinde S, Seabold GK, Mathur P, Davis MI, Bock R, Gustin RM, et al. 2010. Loss of GluN2B-containing NMDA receptors in CA1 hippocampus and cortex impairs long-term depression, reduces dendritic spine density, and disrupts learning. *J Neurosci* **30:** 4590–4600.

Cercato MC, Vázquez CA, Kornisiuk E, Aguirre AI, Colettis N, Snitcofsky M, Jerusalinsky DA, Baez MV. 2017. GluN1 and GluN2A NMDA receptor subunits increase in the hippocampus during memory consolidation in the rat. *Front Behav Neurosci* **10:** 242.

Chen WS, Bear MF. 2007. Activity-dependent regulation of NR2B translation contributes to metaplasticity in mouse visual cortex. *Neuropharmacology* **52:** 200–214.

Chen N, Luo T, Raymond LA. 1999. Subtype-dependence of NMDA receptor channel open probability. *J Neurosci* **19:** 6844–6854.

Commins S, Cunningham L, Harvey D, Walsh D. 2003. Massed but not spaced training impairs spatial memory. *Behav Brain Res* **139:** 215–223.

Cull-Candy S, Brickley S, Farrant M. 2001. NMDA receptor subunits: diversity, development and disease. *Curr Opin Neurobiol* **11:** 327–335.

Dore K, Stein IS, Brock JA, Castillo PE, Zito K, Sjöström PJ. 2017. Unconventional NMDA receptor signaling. *J Neurosci* **37:** 10800–10807.

Number of GluN2 substitutions
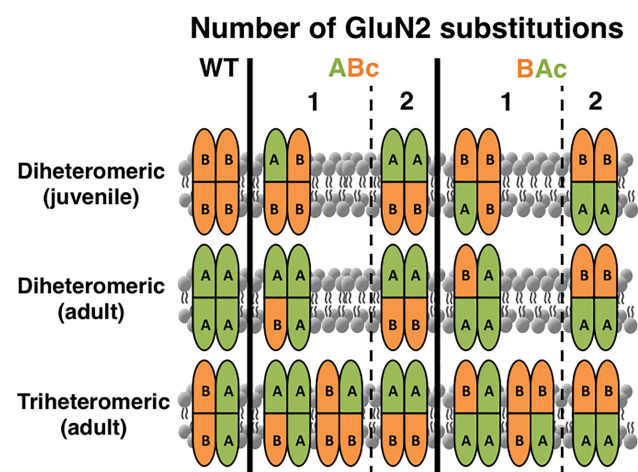
Figure 7. All possible chimeric GluN2 subunit substitution patterns in di- and triheteromeric NMDARs. Synaptic diheteromeric NMDARs containing two GluN2B subunits are lost during postnatal development and replaced by diheteromeric and triheteromeric NMDARs with two GluN2A subunits or one GluN2A and one GluN2B subunit, respectively. Predicted NMDA subunit composition is shown when one or both native GluN2 subunits are replaced by chimeric subunits.

Dumas TC. 2005a. Developmental regulation of cognitive abilities: modified composition of a molecular switch turns on associative learning. *Prog Neurobiol* **76:** 189–211.

Dumas TC. 2005b. Late postnatal maturation of excitatory synaptic transmission permits adult-like expression of hippocampal-dependent behaviors. *Hippocampus* **15:** 562–578.

Elias GM, Elias LA, Apostolides PF, Kriegstein AR, Nicoll RA. 2008. Differential trafficking of AMPA and NMDA receptors by SAP102 and PSD-95 underlies synapse development. *Proc Natl Acad Sci* **105:** 20953–20958.

Erreger K, Dravid SM, Banke TG, Wyllie DJ, Traynelis SF. 2005. Subunit-specific gating controls rat NR1/NR2A and NR1/NR2B NMDA channel kinetics and synaptic signalling profiles. *J Physiol* **563**(Pt 2)**:** 345–358.

Foster KA, McLaughlin N, Edbauer D, Phillips M, Bolton A, Constantine-Paton M, Sheng M. 2010. Distinct roles of NR2A and NR2B cytoplasmic tails in long-term potentiation. *J Neurosci* **30:** 2676–2685.

Fox CJ, Russell KI, Wang YT, Christie BR. 2006. Contribution of NR2A and NR2B NMDA subunits to bidirectional synaptic plasticity in the hippocampus in vivo. *Hippocampus* **16:** 907–915.

Gallagher M, Burwell R, Burchinal M. 1993. Severity of spatial learning impairment in aging: development of a learning index for performance in the Morris Water Maze. *Behav Neurosci* **129:** 540–548.

Gambrill AC, Storey GP, Barria A. 2011. Dynamic regulation of NMDA receptor transmission. *J Neurophysiol* **105:** 162–171.

Gielen M, Retchless BS, Mony L, Johnson JW, Paoletti P. 2009. Mechanism of differential control of NMDA receptor activity by NR2 subunits. *Nature* **459:** 703–707.

Hansel C, de Jeu M, Belmeguenai A, Houtman SH, Buitendijk GH, Andreev D, De Zeeuw CI, Elgersma Y. 2006. α CaMKII is essential for cerebellar LTD and motor learning. *Neuron* **51:** 835–843.

Hayashi T, Thomas GM, Huganir RL. 2009. Dual palmitoylation of NR2 subunits regulates NMDA receptor trafficking. *Neuron* **64:** 213–226.

Izumi Y, Auberson YP, Zorumski CF. 2006. Zinc modulates bidirectional hippocampal plasticity by effects on NMDA receptors. *J Neurosci* **26:** 7181–7188.

Jacobs S, Cui Z, Feng R, Wang H, Wang D, Tsien JZ. 2014. Molecular and genetic determinants of the NMDA receptor for superior learning and memory functions. *PLoS One* **9:** e111865. eCollection.

Jacobs S, Wei W, Wang D, Tsien JZ. 2015. Importance of the GluN2B carboxy-terminal domain for enhancement of social memories. *Learn Mem* **22:** 401–410.

Kapadia M, Xu J, Sakic B. 2016. The water maze paradigm in experimental studies of chronic cognitive disorders: Theory, protocols, analysis, and inference. *Neurosci Biobehav Rev* **68:** 195–217.

Kiyama Y, Manabe T, Sakimura K, Kawakami F, Mori H, Mishina M. 1998. Increased thresholds for long-term potentiation and contextual learning in mice lacking the NMDA-type glutamate receptor ε1 subunit. *J Neurosci* **18:** 6704–6712.

Köhr G, Jensen V, Koester HJ, Mihaljevic AL, Utvik JK, Kvello A, Ottersen OP, Seeburg PH, Sprengel R, Hvalby Ø. 2003. Intracellular domains of NMDA receptor subtypes are determinants for long-term potentiation induction. *J Neurosci* **23:** 10791–10799.

Lau CG, Zukin RS. 2007. NMDA receptor trafficking in synaptic plasticity and neuropsychiatric disorders. *Nat Rev Neurosci* **8:** 413–426.

Li S, Tian X, Hartley DM, Feig LA. 2006. Distinct roles for Ras-guanine nucleotide-releasing factor 1 (Ras-GRF1) and Ras-GRF2 in the induction of long-term potentiation and long-term depression. *J Neurosci* **26:** 1721–1729.

Li LJ, Hu R, Lujan B, Chen J, Zhang JJ, Nakano Y, Cui TY, Liao MX, Chen JC, Man HY, et al. 2016. Glycine potentiates AMPA receptor function through metabotropic activation of GluN2A-containing NMDA receptors. *Front Mol Neurosci* **9:** 102. eCollection.

Lisman J, Schulman H, Cline H. 2002. The molecular basis of CaMKII function in synaptic and behavioural memory. *Nat Rev Neurosci* **3:** 175–190.

Liu L, Wong TP, Pozza MF, Lingenhoehl K, Wang Y, Sheng M, Auberson YP, Wang YT. 2004. Role of NMDA receptor subtypes in governing the direction of hippocampal synaptic plasticity. *Science* **304:** 1021–1024.

Malenka RC, Bear MF. 2004. LTP and LTD: an embarrassment of riches. *Neuron* **44:** 5–21.

Massey PV, Johnson BE, Moult PR, Auberson YP, Brown MW, Molnar E, Collingridge GL, Bashir ZI. 2004. Differential roles of NR2A and NR2B-containing NMDA receptors in cortical long-term potentiation and long-term depression. *J Neurosci* **24:** 7821–7828.

Mayford M, Wang J, Kandel ER, O'Dell TJ. 1995. CaMKII regulates the frequency-response function of hippocampal synapses for the production of both LTD and LTP. *Cell* **81:** 891–904.

Mayford M, Bach ME, Huang YY, Wang L, Hawkins RD, Kandel ER. 1996. Control of memory formation through regulated expression of a CaMKII transgene. *Science* **274:** 1678–1683.

Merrill MA, Chen Y, Strack S, Hell JW. 2005. Activity-driven postsynaptic translocation of CaMKII. *Trends Pharmacol Sci* **26:** 645–653.

Minatohara K, Ichikawa SH, Seki T, Fujiyoshi Y, Doi T. 2013. Ligand binding of PDZ domains has various roles in the synaptic clustering of SAP102 and PSD-95. *Neurosci Lett* **533:** 44–49.

Monyer H, Sprengel R, Schoepfer R, Herb A, Higuchi M, Lomeli H, Burnashev N, Sakmann B, Seeburg PH. 1992. Heteromeric NMDA receptors: molecular and functional distinction of subtypes. *Science* **256:** 1217–1221.

Monyer HN, Burnashev DJ, Laurie, Sakmann B, Seeburg PH. 1994. Developmental and regional expression in the rat brain and functional properties of four NMDA receptors. *Neuron* **12:** 529–540.

Mullasseril P, Hansen KB, Vance KM, Ogden KK, Yuan H, Kurtkaya NL, Santangelo R, Orr AG, Le P, Vellano KM, Liotta DC, et al. 2010. A subunit-selective potentiator of NR2C- and NR2D-containing NMDA receptors. *Nat Commun* **1:** 90.

Nabavi S, Kessels HW, Alfonso S, Aow J, Fox R, Malinow R. 2013. Metabotropic NMDA receptor function is required for NMDA receptor-dependent long-term depression. *Proc Natl Acad Sci* **110:** 4027–4032.

Newpher TM, Ehlers MD. 2009. Spine microdomains for postsynaptic signaling and plasticity. *Trends Cell Biol* **19:** 218–227.

Pachernegg S, Strutz-Seebohm N, Hollmann M. 2012. GluN3 subunit-containing NMDA receptors: not just one-trick ponies. *Trends Neurosci* **35:** 240–249.

Paoletti P, Neyton J. 2007. NMDA receptor subunits: function and pharmacology. *Cur Opin Pharmacol* **7:** 39–47.

Paylor R, Baskall-Baldini L, Yuva L, Wehner JM. 1996. Developmental differences in place-learning performance between C57BL/6 and DBA/2 mice parallel the ontogeny of hippocampal protein kinase C. *Behav Neurosci* **110:** 1415–1425.

Pereira T, Burwell R. 2015. Using the spatial learning index to evaluate performance on the water maze. *Behav Neurosci* **129:** 533–539.

Petralia RS, Al-Hallaq RA, Wenthold RJ. 2009. Trafficking and Targeting of NMDA Receptors. In *Biology of the NMDA receptor*. Chapter 8. (ed. Van Dongen AM). CRC Press/Taylor & Francis, Boca Raton, FL.

Pi HJ, Otmakhov N, Lemelin D, De Koninck P, Lisman J. 2010. Autonomous CaMKII can promote either long-term potentiation or long-term depression, depending on the state of T305/T306 phosphorylation. *J Neurosci* **30:** 8704–8709.

Prybylowski K, Chang K, Sans N, Kan L, Vicini S, Wenthold RJ. 2005. The synaptic localization of NR2B-containing NMDA receptors is controlled by interactions with PDZ proteins and AP-2. *Neuron* **47:** 845–857.

Rauner C, Köhr G. 2011. Triheteromeric NR1/NR2A/NR2B receptors constitute the major N-methyl-D-aspartate receptor population in adult hippocampal synapses. *J Biol Chem* **286:** 7558–7566.

Rudy JW, Stadler-Morris S, Albert P. 1987. Ontogeny of spatial navigation behaviors in the rat: dissociation of "proximal"- and "distal"-cue-based behaviors. *Behav Neurosci* **101:** 62–73.

Ryan TJ, Kopanitsa MV, Indersmitten T, Nithiananantharajah J, Afinowi NO, Pettit C, Stanford LE, Sprengel R, Saksida LM, Bussey TJ, et al. 2013. Evolution of GluN2A/B cytoplasmic domains diversified vertebrate synaptic plasticity and behavior. *Nat Neurosci* **16:** 25–32.

Sakimura K, Kutsuwada T, Ito I, Manabe T, Takayama C, Kushiya E, Yagi T, Aizawa S, Inoue Y, Sugiyama H, et al. 1995. Reduced hippocampal LTP and spatial learning in mice lacking NMDA receptor ε1 subunit. *Nature* **373:** 151–155.

Sala C, Sheng M. 1999. The fyn art of *N*-methyl-D-aspartate receptor phosphorylation. *Proc Natl Acad Sci* **96:** 335–337.

Sanders EM, Nguyen MA, Zhou KC, Hanks ME, Yusuf KA, Cox DN, Dumas TC. 2013. Developmental modification of synaptic NMDAR composition and maturation of glutamatergic synapses: matching postsynaptic slots with receptor pegs. *Biol Bull* **224:** 1–13.

Sanhueza M, Lisman J. 2013. The CaMKII/NMDAR complex as a molecular memory. *Mol Brain* **6:** 10.

Sans N, Petralia RS, Wang YX, Blahos J 2nd, Hell JW, Wenthold RJ. 2000. A developmental change in NMDA receptor-associated proteins at hippocampal synapses. *J Neurosci* **20:** 1260–1271.

Sans N, Prybylowski K, Petralia RS, Chang K, Wang YX, Racca C, Vicini S, Wenthold RJ. 2003. NMDA receptor trafficking through an interaction between PDZ proteins and the exocyst complex. *Nat Cell Biol* **5:** 520–530.

Sheng M. 2001. The postsynaptic NMDA-receptor--PSD-95 signaling complex in excitatory synapses of the brain. *J Cell Sci* **114**(Pt 7)**:** 1251.

Shinohara K, Hata T. 2018. Post-acquisition hippocampal blockade of the NMDA receptor subunit GluN2A but not GluN2B sustains spatial reference memory retention. *Neurobiol Learn Mem* **147:** 1–8.

Sprengel R, Suchanek B, Amico C, Brusa R, Burnashev N, Rozov A, Hvalby O, Jensen V, Paulsen O, Andersen P, et al. 1998. Importance of the

intracellular domain of NR2 subunits for NMDA receptor function in vivo. *Cell* **92:** 279–289.

Stein LR, Zorumski CF, Imai S, Izumi Y. 2015. Nampt is required for long-term depression and the function of GluN2B subunit-containing NMDA receptors. *Brain Res Bull* **119**(Pt A)**:** 41–51.

Stoneham ET, Sanders EM, Sanyal M, Dumas TC. 2010. Rules of engagement: factors that regulate activity-dependent synaptic plasticity during neural network development. *Biol Bull* **219:** 81–99.

Tang YP, Shimizu E, Dube GR, Rampon C, Kerchner GA, Zhuo M, Liu G, Tsien JZ. 1999. Genetic enhancement of learning and memory in mice. *Nature* **401:** 63–69.

Travaglia A, Bisaz R, Cruz E, Alberini CM. 2016. Developmental changes in plasticity, synaptic, glia and connectivity protein levels in rat dorsal hippocampus. *Neurobiol Learn Mem* **135:** 125–138.

Vissel B, Krupp JJ, Heinemann SF, Westbrook GL. 2001. A use-dependent tyrosine dephosphorylation of NMDA receptors is independent of ion flux. *Nat Neurosci* **4:** 587–596.

von Engelhardt J, Doganci B, Jensen V, Hvalby Ø, Göngrich C, Taylor A, Barkus C, Sanderson DJ, Rawlins JN, Seeburg PH, et al. 2008. Contribution of hippocampal and extra-hippocampal NR2B-containing NMDA receptors to performance on spatial learning tasks. *Neuron* **60:** 846–860.

Vorhees CV, Williams MT. 2014. Assessing spatial learning and memory in rodents. *ILAR J* **55:** 310–332.

Wang CC, Held RG, Chang SC, Yang L, Delpire E, Ghosh A, Hall BJ. 2011. A critical role for GluN2B-containing NMDA receptors in cortical development and function. *Neuron* **72:** 789–805.

Yuan H, Hansen KB, Vance KM, Ogden KK, Traynelis SF. 2009. Control of NMDA receptor function by the NR2 subunit amino-terminal domain. *J Neurosci* **29:** 12045–12058.